Optically Addressable Silicon Vacancy-Related Spin Centers in Rhombic Silicon Carbide with High Breakdown Characteristics and ENDOR Evidence of Their Structure

V. A. Soltamov,[1,*] B. V. Yavkin,[2] D. O. Tolmachev,[1] R. A. Babunts,[1] A. G. Badalyan,[1] V. Yu. Davydov,[1] E. N. Mokhov,[1] I. I. Proskuryakov,[3] S. B. Orlinskii,[2] and P. G. Baranov[1]

[1]*Ioffe Physical Technical Institute, St. Petersburg 194021, Russia*

[2]*Kazan Federal University, Kazan 420008, Russia*

[3]*Institute of Basic Biological Problems RAS, Pushchino 142290, Russia*

(Received 16 June 2015; revised manuscript received 20 September 2015; published 11 December 2015)

We discovered a family of uniaxially oriented silicon vacancy-related centers with $S = 3/2$ in a rhombic 15R-SiC crystalline matrix. We demonstrate that these centers exhibit unique characteristics such as optical spin alignment up to the temperatures of 250 °C. Thus, the range of robust optically addressable vacancy-related spin centers is extended to the wide class of rhombic SiC polytypes. To use these centers for quantum applications it is essential to know their structure. Using high frequency electron nuclear double resonance, we show that the centers are formed by negatively charged silicon vacancies V_{Si}^- in the paramagnetic state with $S = 3/2$ that is noncovalently bonded to the neutral carbon vacancy V_C^0 in the nonparamagnetic state, located on the adjacent site along the SiC symmetry c axis.

DOI: 10.1103/PhysRevLett.115.247602 PACS numbers: 76.70.Hb, 61.72.Hh, 76.30.Mi, 76.70.Dx

Spin centers in silicon carbide (SiC) have recently been put forward as favorable candidates for quantum spintronics, sensorics, and quantum information processing because of the unique properties of their electron spins, which can be optically polarized and read out [1–11]. Optical control of the spin states of the single defect was realized on the well studied V_{Si}^--related center with ground spin state $S = 3/2$ in 4H-SiC [10]. Similar centers also exist in 6H-SiC polytype and can be used in quantum magnetometry [6] and masers [8]. Pronounced semiconducting properties of SiC allow one to fabricate an effective p-n junction, thus allowing the electrical readout of the V_{Si}^- spin state [12].

The first solid state system on which optical detection and manipulation of the single spin was shown is the negatively charged nitrogen-vacancy (NV^-) center in diamond. Control of the single spins became possible because NV^- centers possess high optically detected magnetic resonance (ODMR) contrast and their spin alignment persists at elevated temperatures [13,14]. A precise atomic structure of the center was elucidated [15,16], enabling controllable fabrication of NV^- centers with a desired topology [17,18]. This allows one to control interactions between electron spins of the centers and the environment, which is a basis for NV^--based quantum registers [19,20] and quantum sensors [21,22].

Therefore, for the successful development of SiC-based applications, two major issues have to be addressed: exploration of the spin centers with high breakdown characteristics and identification of the microscopic model of these spin centers. We focused our efforts on these two tasks.

We used SiC single crystals of 15R polytype that were grown by the physical vapor transport method. The concentration of uncompensated nitrogen was $\approx 10^{16}$ cm^{-3}. Vacancies were created by irradiation of the crystals with 1.4 MeV electrons with a fluence of 10^{18} cm^{-2}. The crystal structure was confirmed by Raman spectroscopy and presented in the Supplemental Material [23,27,28].

First, we characterized 15R-SiC samples by measuring photoluminescence (PL) and continuous wave X-band (≈9.3 GHz) electron paramagnetic resonance (EPR). The PL spectrum was recorded under continuous illumination at $\lambda = 532$ nm, $T = 10$ K, and it exhibits four zero phonon lines (ZPL) that we labeled as $V1$–$V4$ [Fig. 1(a), Table I]. EPR spectra [Fig. 1(b)] were recorded under continuous light illumination at $\lambda = 785$ nm. The magnetic field was oriented parallel to the c axis of the crystal ($B \| c$). Without optical excitation the signals were near the noise threshold. Under optical excitation, EPR signals were clearly observable up to the temperature $T = 250$ °C. EPR spectra consist of three pairs of transitions labeled $V2$, $V3$, $V4$. To determine the correspondence between PL and EPR spectra we used resonant optical excitation at the ZPL wavelength and measure the time resolved EPR response (see the Supplemental Material [23]). All $V1$–$V4$ centers in 15R-SiC have their own optical fingerprint; however, resonant excitation into the $V1$ line ($\lambda = 863.2$ nm) did not give rise to the EPR signal; thus, the $V1$ center is EPR silent and we do not discuss it in what follows. For each of the $V2$, $V3$, $V4$ signals we observed phase reversal for one of the two transitions in each pair of lines. Such behavior in the emission or absorption mode of the microwave power can be explained by induced spin alignment of the spin sublevels of the centers under optical excitation.

To determine the symmetry of the centers, we measured angular dependencies (see the Supplemental Material [23]),

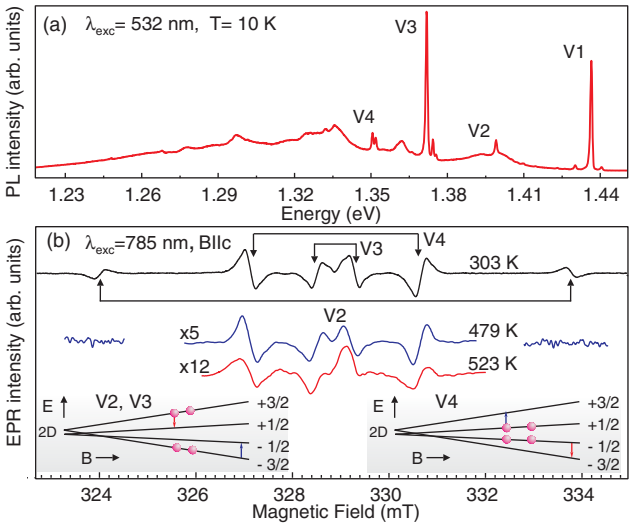

FIG. 1 (color online). (a) PL spectrum of the V_{Si}^--related centers in 15R-SiC. (b) EPR spectra measured at temperatures $T = 303$ K, $T = 479$ K, $T = 523$ K. The insets show the light-induced inverse population of the spin sublevels of $V2$, $V3$, and $V4$ centers.

that can be fitted well by spin Hamiltonian with parameters summarized in Table I:

$$H = g\mu_B \vec{B}_0 \cdot \vec{S} + D\left[S_Z^2 - \frac{1}{3}S(S+1)\right], \qquad (1)$$

where the first and the second terms correspond to the Zeeman interaction and fine structure splitting, respectively, μ_B is the Bohr magneton, g is electron g factor, and S_Z is the projection of the total spin on the symmetry axis of the center. Without an external magnetic field ($B = 0$) the ground state is split due to the presence of the crystal field D and for $S = 3/2$ spin state the zero-field splitting (ZFS) between $M_S = \pm 1/2$ and $M_S = \pm 3/2$ sublevels is equal to $2D$. The spin state $S = 3/2$ is confirmed by ODMR measurements that we discuss later. Observed angular dependencies show that all three centers are oriented along the c axis and have C_{3v} point-group symmetry.

The optical polarization of observed centers can be created at high temperatures up to $T \approx 250$ °C. This indicates that the spin system is well isolated from the crystalline lattice vibration. In this aspect, these centers are similar to the NV$^-$ centers in diamond, with one important distinction—the ZFS of each $V2$, $V3$, and $V4$ center is stable over the whole temperature range, while for the NV$^-$ centers, a huge thermal shift was observed [13,29,30].

To establish the optical polarization scheme of the $V2$, $V3$, and $V4$ centers we used high frequency W-band (94 GHz) electron spin echo detected EPR (ESE) and electron nuclear double resonance (ENDOR). We determined that ZFS is positive for each center, and established the scheme of the optically polarized spin sublevels (see the Supplemental Material [23]). Optical polarization schemes for $V2$, $V3$ centers and for the $V4$ center are different, and are shown in Fig. 1 (inset).

Another important characteristic is the coherence time of the spin centers, which we measured using a pulsed X-band EPR technique (see the Supplemental Material [23]). Spin lattice relaxation times (T_1) and spin-spin relaxation times (T_2) are summarized in Table I. Spin-spin relaxation times are shorter than $T_2 = 120$ μs reported for the single V_{Si}^--related center in 4H-SiC [10]. The main mechanism leading to the decoherence seems to be a dipole-dipole interaction between the paramagnetic spin centers created by irradiation [31]. In Ref. [10] the vacancies were created in the high purity 4H-SiC sample by irradiation with a low fluence of electrons ($< 5 \times 10^{14}$ cm^{-2}).

We further demonstrate that the V_{Si}^--related centers in 15R-SiC can be optically addressed and read-out with high fidelity at room temperature by means of standard ODMR.

The ODMR spectrum shows the relative change of the photoluminescence intensity ΔPL/PL as a function of applied radio frequency (Fig. 2). Resonances at $\nu = 13.1$ MHz, $\nu = 50.6$ MHz, and $\nu = 138$ MHz were observed and agree with ZFS of the $V3$, $V4$, and $V2$ centers determined from our EPR measurements.

Using the spin Hamiltonian from Eq. (1), we calculated that the ground states of the centers have a spin state $S = 3/2$. Calculated frequency dependencies of the ODMR signals at different strengths of magnetic fields ($B \| c$) coincided well with observed spectra (Fig. 2). We believe that changing the excitation energy and the optical registration window can lead to the further increase of the ODMR contrast. We made trial measurements of $V4$ ODMR signals in 15R-SiC under laser excitation at $\lambda = 808$ nm, and observed about five times more intense signals than for the similar centers in other polytypes (1.2% for $V4$ centers).

In order to advance our understanding of the observed spin system and to foster its usability we suggest the microscopic model of the centers. Currently, two possible models are under consideration for analog centers in hexagonal SiC polytypes. The first model suggests that the V_{Si}^--related centers are the low symmetry configuration of the V_{Si}^- with $S = 3/2$ [32,33]. The second model suggests that these centers are the V_{Si}^- with $S = 3/2$, perturbed by the presence of the neutral carbon vacancy V_C^0 in the nonparamagnetic state, located adjacently to the V_{Si}^- along the c axis [8].

TABLE I. ZPLs wavelength, values of D, g, and T_1, T_2 relaxation times measured at room temperature.

Center	ZPL (nm)	D (MHz)	g	T_1 μs	T_2 μs
$V2$	886.5	69.6 ± 1	2.005(1)	80	10
$V3$	904	5.8 ± 1	2.005(3)	120	10
$V4$	917	25.1 ± 1	2.005(3)	105	9

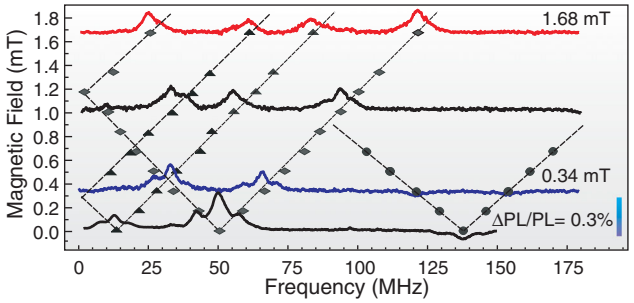

FIG. 2 (color online). The lower spectrum shows the ODMR signal of the $V2$, $V3$, $V4$ detected under laser excitation $\lambda = 785$ nm in the 0.05 mT external magnetic field applied to compensate the influence of Earth's magnetic field. the vertical bar indicates the ODMR contrast. Experimental frequency dependence of the ODMR signals as a function of magnetic field are shown for each center. Dashed lines are the calculated dependence using Eq. (1).

In what follows we discuss ESE and ENDOR spectra measured in 15R-SiC (Fig. 3), and show that observed Hyperfine (HF) interactions strongly evidence in favor of the second model, i.e., the $V_{Si}^- - V_C^0$ model with $S = 3/2$. The microscopic structure of the center is shown in Fig. 4.

To begin, we measured W-band ESE spectra of the $V2$, $V3$, and $V4$ centers for two orientations (θ) of the magnetic field B with respect to the c axis [Fig. 3(a)]. Similarly to the case of 4H-SiC and 6H-SiC, we observed two types of HF interactions in the ESE spectra. The first type of the HF interactions occurs with the ^{13}C nucleus located in the nearest neighbor (NN) shell to the V_{Si}^- site. They are strongly anisotropic and reflect the tetrahedral symmetry of the nuclear spin locations. The HF lines arising from these interactions are shown in Fig. 3(a): $^{13}C_1$ denotes the interaction with the carbon atom oriented along the c axis and $^{13}C_{2-4}$ denotes the interactions with atoms located in the basal plane with the bonds inclined by the angle $\theta = 71°$ relative to the c axis. The HF structure arising from such interactions is characterized by $A_{\parallel} = 30.2$ G (84.6 MHz) and $A_{\perp} = 12$ G (33.6 MHz), which match closely previously reported values for the V_{Si}^- centers in 4H-SiC and 6H-SiC [34–37]. The second type of the HF interactions occurs with the ^{29}Si nucleus located in the next nearest neighbor (NNN) shell to the V_{Si}^-. These interactions with $A = 2.97$ G are shown in the inset in Fig. 3(a). Changes in the orientation of the magnetic field did not induce the line shifts; only the strong anisotropy of the linewidth was observed.

Our discussion is based on the ENDOR spectra of the $V2$ centers. Figures 3(b) and 3(c) show the ENDOR spectra recorded by monitoring the intensity of the ESE, following microwave $\pi/2$ pulses, as a frequency function of the pulse, applied between the second and third microwave pulses [38]. Allowed dipole magnetic transitions with $\Delta M_S = \pm 1 : 3/2 \leftrightarrow 1/2$ are indicated by lf (low field) and $-3/2 \leftrightarrow -1/2$ are indicated by hf (high field).

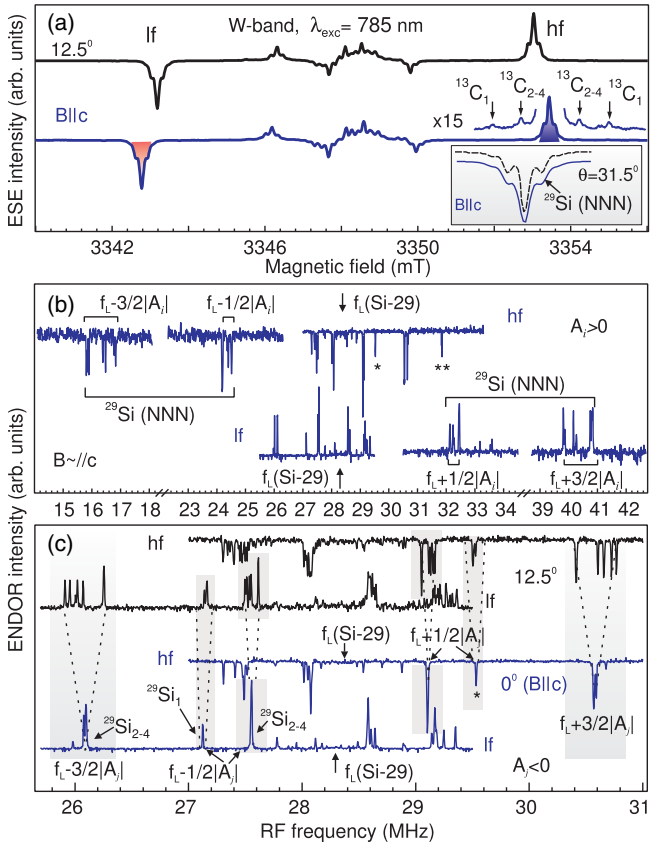

FIG. 3 (color online). (a) Optically induced ESE spectra measured at two angles θ between the B and c axis: $\theta = 0°$ and $\theta = 12.5°$. (b),(c) ENDOR spectra measured for the lf and hf transitions indicated in (a). Transitions corresponding to the $f_L + 1/2|A_j|$ and $f_L + 3/2|A_j|$ for HF interactions with the axial NN Si atom with respect to V_C^0 are indicated by one and two asterisks, respectively. $^{29}Si_1$ and $^{29}Si_{2-4}$ indicate ENDOR lines corresponding to the presence of ^{29}Si atoms in the NN shell of the V_C^0.

Observed HF interactions with silicon and carbon nuclei can be described by adding $\Sigma \mathbf{S} A_i \mathbf{I}_i + \Sigma \mathbf{S} A_j \mathbf{I}_j + \Sigma \mathbf{S} A_k \mathbf{I}_k$ terms to the spin Hamiltonian [Eq. (1)]. Here, $\mathbf{A}_i$ and $\mathbf{A}_k$ are tensors, which describe the HF interaction with the ith Si and kth C atoms located at different neighbor shells of the Si sites, $\mathbf{A}_j$ is a tensor that describes the HF interaction with the jth Si atoms located at different neighbor shells of the C sites.

ENDOR transition frequencies determined by the selection rules $\Delta M_S = 0$ and $\Delta M_I = \pm 1$ are given by [39]:

$$\nu_{\mathrm{ENDOR}i} = h^{-1} |M_S [a_i + b_i (3\cos^2\theta - 1)] - g_{ni}\mu_n B|, \qquad (2)$$

where a_i and b_i are isotropic and anisotropic parts of the HF interaction with the ith nucleus, θ is the angle between the external magnetic field B and the HF interaction tensor, $g_{ni}\mu_{ni}B/h$ is the Larmor frequency f_L, g_{ni}, and μ_{ni} are the g factor of nucleus i and its Bohr magneton (g_n is negative for ^{29}Si and positive for ^{13}C). For axial symmetry the HF

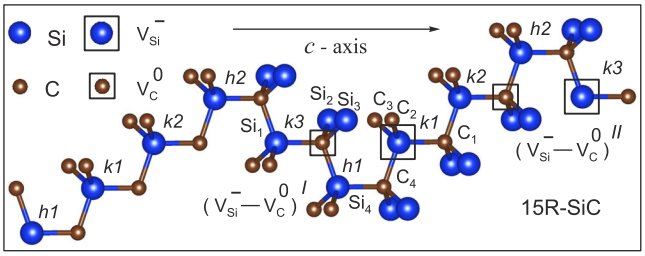

FIG. 4 (color online). The 15R-SiC structure with two hexgonal ($h1$, $h2$) and three quasicubic ($k1$, $k2$, $k3$) sites for silicon. Vacancies are shown as squares. Carbon and silicon atoms in the NN shell of the V_{Si}^- and V_C^0 are labeled as C_{1-4} and Si_{1-4}, respectively. The structure of the $V2$ center is indicated as $(V_{Si}^- - V_C^0)\prime$, and $(V_{Si}^- - V_C^0)\prime\prime$.

interaction in terms of the principal values is given by $A_\parallel = a + 2b$, $A_\perp = a - b$.

All lines observed in the spectra in Fig. 3(b) can be attributed to the HF interactions between V_{Si}^- electron spin and ^{29}Si nuclear spin. To reveal this, we need to consider Eq. (2), which predicts that interaction with each ith nucleus induces two sets of ENDOR transitions located at the distances of $3/2A_i$ and $1/2A_i$ for the lf EPR line, $-3/2A_i$ and $-1/2A_i$ for the hf EPR line, from the Larmor frequency f_L. Thus, the ENDOR lines observed are due to the HF interactions with ^{29}Si, because the f_L of the ^{29}Si ($I = 1/2$, abundance 4.7%) is about 28.2 MHz [marked by arrows in Figs. 3(b) and 3(c)]. HF interactions of the V_{Si}^- electron spin with ^{29}Si nuclear magnetic moments in the NNN shell observed in the ESE spectra can also be seen in the ENDOR spectra [Fig. 3(b)], labeled ^{29}Si (NNN). The position of these lines corresponds to the positive spin density of the electronic wave function on the silicon nucleus.

Unexpectedly, we also observed ENDOR signals that arose due to the negative spin density on the Si nucleus. These strongly anisotropic signals labeled as $^{29}Si_1$ and $^{29}Si_{2-4}$ are shown in Fig. 3(c). As discussed earlier, interactions between V_{Si}^- and ^{29}Si located in NNN and more distant shells are almost isotropic, meanwhile, interactions with ^{13}C located in the NN shell are anisotropic. In the ENDOR spectra the HF interactions characterized by the negative spin density on ^{29}Si exhibit anisotropic dependence typical of the HF interactions between ^{13}C located in the NN shell and V_{Si}^-. To explain such anisotropy, we need to identify Si atoms that have the same symmetry as the C atoms. Such a configuration can be found only at the tetrahedron vertices around the carbon site. The position of the ENDOR lines labeled as $^{29}Si_1$ and $^{29}Si_{2-4}$ in Fig. 3(c) agrees well with the proposed configuration and reflects the HF interactions with axial (Si_1) and basal (Si_{2-4}) nuclear spins (Fig. 4). The line corresponding to the HF interactions with axially oriented Si nuclei for transitions with $M_S = 3/2$ is marked in Fig. 3(b) by two asterisks. The constants of the HF interactions are relatively large $A_\parallel = 2.2$ MHz (≈0.8 G) and $A_\perp = 1.3$ MHz (≈0.5 G) and describe well the anisotropy of the linewidth observed in the ESE.

These HF interactions characterized by the negative spin density on the ^{29}Si nuclei can be explained if the spin density is located on four Si nuclei placed around nonparamagnetic neutral V_C^0. This implies that the $V2$ center is formed by both nonparamagnetic V_C^0 and paramagnetic $S = 3/2$ V_{Si}^-. Negative spin density is caused by the spin polarization (similar to the core polarization for transition metals [40,41]), and arises from an exchange interaction with $S = 3/2$ that leads to the partial decoupling of coupled covalent bonds of the V_C^0 site. The presence of the V_C^0 distorts the crystal lattice, which in turn lowers the symmetry of the V_{Si}^-. Because the $V2$ center is characterized by the largest ZFS we can conclude that V_{Si}^- and V_C^0 are located closer to each other than in the case of $V3$, $V4$ centers.

The duplication of lines observed in the ENDOR spectra can be explained by the presence of two similar centers with slightly different parameters of the HF interactions. Based on our experiments we suggested the model of the $V2$ centers shown in Fig. 4. The model represents two possible configurations $(V_{Si}^- - V_C^0)\prime$, and $(V_{Si}^- - V_C^0)\prime\prime$, depending on the positions of the vacancies in the lattice.

In conclusion, we studied three optically addressable vacancy-related centers in 15R-SiC. These centers with distinct ZPL and ZFS were characterized by long spin coherence times at room temperature and strong ODMR contrast. Their optical spin alignment persisted up to 250 °C. The ENDOR studies allowed us to determine the model of the V_{Si}^--related centers. This knowledge is important for understanding the processes leading to decoherence [42] and effective and precise production of V_{Si}^--related centers. The presented results extend the concept of optically addressable V_{Si}^--related centers to the rhombic polytypes of SiC, and pave the way for SiC-based quantum applications and quantum registers based on coupled electron spins in 15R-SiC.

This work was funded by the Ministry of Education and Science of the Russian Federation No. 14.604.21.0083 (RFMEFI60414X0083) and by the RFBR No. 13-02-00821.

*victrosoltamov@gmail.com

[1] P. G. Baranov, A. P. Bundakova, I. V. Borovykh, S. B. Orlinskii, R. Zondervan, and J. Schmidt, JETP Lett. **86**, 202 (2007).
[2] P. G. Baranov, A. P. Bundakova, A. A. Soltamova, S. B. Orlinskii, I. V. Borovykh, R. Zondervan, R. Verberk, and J. Schmidt, Phys. Rev. B **83**, 125203 (2011).
[3] V. A. Soltamov, A. A. Soltamova, P. G. Baranov, and I. I. Proskuryakov, Phys. Rev. Lett. **108**, 226402 (2012).

[4] W. F. Koehl, B. B. Buckley, F. J. Heremans, G. Calusine, and D. D. Awschalom, Nature (London) **479**, 84 (2011).
[5] A. L. Falk, B. B. Buckley, G. Calusine, W. F. Koehl, V. V. Dobrovitski, A. Politi, C. A. Zorman, P. X.-L. Feng, and D. D. Awschalom, Nat. Commun. **4**, 1819 (2013).
[6] H. Kraus, V. A. Soltamov, F. Fuchs, D. Simin, A. Sperlich, P. G. Baranov, G. V. Astakhov, and V. Dyakonov, Sci. Rep. **4**, 5303 (2014).
[7] A. L. Falk, P. V. Klimov, B. B. Buckley, V. Ivády, I. A. Abrikosov, G. Calusine, W. F. Koehl, Á. Gali, and D. D. Awschalom, Phys. Rev. Lett. **112**, 187601 (2014).
[8] H. Kraus, V. A. Soltamov, D. Riedel, S. Väth, F. Fuchs, A. Sperlich, P. G. Baranov, V. Dyakonov, and G. V. Astakhov, Nat. Phys. **10**, 157 (2014).
[9] P. V. Klimov, A. L. Falk, B. B. Buckley, and D. D. Awschalom, Phys. Rev. Lett. **112**, 087601 (2014).
[10] M. Widmann, S.-Y. Lee, T. Rendler, N. T. Son, H. Fedder, S. Paik, L.-P. Yang, N. Zhao, S. Yang, I. Booker, A. Denisenko, M. Jamali, S. A. Momenzadeh, I. Gerhardt, T. Ohshima, A. Gali, E. Janzén, and J. Wrachtrup, Nat. Mater. **14**, 164 (2015).
[11] D. J. Christle, A. L. Falk, P. Andrich, P. V. Klimov, J. Hassan, N. T. Son, E. Janzén, T. Ohshima, and D. D. Awschalom, Nat. Mater. **14**, 160 (2015).
[12] C. J. Cochrane, P. M. Lenahan, and A. J. Lelis, Appl. Phys. Lett. **100**, 023509 (2012).
[13] D. M. Toyli, D. J. Christle, A. Alkauskas, B. B. Buckley, C. G. Van de Walle, and D. D. Awschalom, Phys. Rev. X **2**, 031001 (2012).
[14] A. Gruber, A. Draübenstedt, C. Tietz, L. Fleury, J. Wrachtrup, and C. Borczyskowski, Science **276**, 2012 (1997).
[15] J. H. N. Loubser and J. A. van Wyk, Rep. Prog. Phys. **41**, 1201 (1978).
[16] D. A. Redman, S. Brown, R. H. Sands, and S. C. Rand, Phys. Rev. Lett. **67**, 3420 (1991).
[17] J. Martin, R. Wannemacher, J. Teichert, L. Bischoff, and B. Kohler, Appl. Phys. Lett. **75**, 3096 (1996).
[18] S. Pezzagna, D. Wildanger, P. Mazarov, A. D. Wieck, Y. Sarov, I. Rangelow, B. Naydenov, F. Jelezko, S. W. Hell, and J. Meijer, Small **6**, 2117 (2010).
[19] G. Waldherr, Y. Wang, S. Zaiser, M. Jamali, T. Schulte-Herbrüggen, H. Abe, T. Ohshima, J. Isoya, J. F. Du, P. Neumann, and J. Wrachtrup, Nature (London) **506**, 204 (2014).
[20] T. H. Taminiau, J. Cramer, T. van der Sar, V. V. Dobrovitski, and R. Hanson, Nat. Nanotechnol. **9**, 171 (2014).
[21] V. M. Acosta, E. Bauch, M. P. Ledbetter, C. Santori, K.-M. C. Fu, P. E. Barclay, R. G. Beausoleil, H. Linget, J. F. Roch, F. Treussart, S. Chemerisov, W. Gawlik, and D. Budker, Phys. Rev. B **80**, 115202 (2009).
[22] F. Dolde, M. W. Doherty, J. Michl, I. Jakobi, B. Naydenov, S. Pezzagna, J. Meijer, P. Neumann, F. Jelezko, N. B. Manson, and Jörg Wrachtrup, Phys. Rev. Lett. **112**, 097603 (2014).
[23] See Supplemental Material at http://link.aps.org/supplemental/10.1103/PhysRevLett.115.247602, which includes Refs. [24–26], for additional data and experimental details.
[24] Th. Lingner, S. Greulich-Weber, J.-M. Spaeth, U. Gerstmann, E. Rauls, Z. Hajnal, Th. Frauenheim, and H. Overhof, Phys. Rev. B **64**, 245212 (2001).
[25] P. G. Baranov, I. V. Ilin, E. N. Mokhov, M. V. Muzafarova, S. B. Orlinskii, and J. Schmidt, JETP Lett. **82**, 441 (2005).
[26] S. Stoll and A. Schweiger, J. Magn. Reson. **178**, 42 (2006).
[27] S. Nakashima and H. Harima, Phys. Status Solidi (a) **162**, 39 (1997).
[28] D. W. Feldman, J. H. Parker, Jr., W. J. Choyke, and L. Patrick, Phys. Rev. **170**, 698 (1968).
[29] V. M. Acosta, E. Bauch, M. P. Ledbetter, A. Waxman, L.-S. Bouchard, and D. Budker, Phys. Rev. Lett. **104**, 070801 (2010).
[30] R. A. Babunts, A. A. Soltamova, D. O. Tolmachev, V. A. Soltamov, A. S. Gurin, A. N. Anisimov, V. L. Preobrazhenskii, and P. G. Baranov, JETP Lett. **95**, 429 (2012).
[31] See Supplemental Material to M. Widmann, S.-Y. Lee, T. Rendler, N. T. Son, H. Fedder, S. Paik, L.-P. Yang, N. Zhao, S. Yang, I. Booker, A. Denisenko, M. Jamali, S. A. Momenzadeh, I. Gerhardt, T. Ohshima, A. Gali, E. Janzén, and J. Wrachtrup, Nat. Mater. **14**, 164 (2015).
[32] N. Mizuochi, S. Yamasaki, H. Takizawa, N. Morishita, T. Ohshima, H. Itoh, T. Umeda, and J. Isoya, Phys. Rev. B **72**, 235208 (2005).
[33] E. Janzén, A. Gali, P. Carlsson, A. Gällström, B. Magnusson, and N. T. Son, Physica (Amsterdam) **404B**, 4354 (2009).
[34] H. J. von Bardeleben, J. L. Cantin, I. Vickridge, and G. Battistig, Phys. Rev. B **62**, 10126 (2000).
[35] T. Wimbauer, B. K. Meyer, A. Hofstaetter, A. Scharmann, and H. Overhof, Phys. Rev. B **56**, 7384 (1997).
[36] N. Mizuochi, S. Yamasaki, H. Takizawa, N. Morishita, T. Ohshima, H. Itoh, and J. Isoya, Phys. Rev. B **66**, 235202 (2002).
[37] W. E. Carlos, N. Y. Garces, E. R. Glaser, and M. A. Fanton, Phys. Rev. B **74**, 235201 (2006).
[38] W. B. Mims, in *Electron Paramagnetic Resonance*, edited by S. Geschwind (Plenum, New York, 1972).
[39] J.-M. Spaeth, J. R. Niklas, and R. H. Bartram, *Structural Analysis of Point Defects in Solids* (Springer-Verlag, Berlin, Heidelberg, 1992), Chap. 5, p. 152.
[40] A. J. Freeman and R. B. Frankel, *Hyperfine Interactions* (Academic Press, New York, London, 1967).
[41] A. Abraham and B. Bleaney, *Electron Paramagnetic Resonance of Transition Ions* (Clarendon Press, Oxford, 1970), p. 702.
[42] Li-Ping Yang, Christian Burk, Matthias Widmann, Sang-Yun Lee, Jörg Wrachtrup, and Nan Zhao, Phys. Rev. B **90**, 241203(R) (2014).